Journal of Power Sources 196 (2011) 5215–5222

Contents lists available at ScienceDirect

Journal of Power Sources

journal homepage: www.elsevier.com/locate/jpowsour

Capacitance studies of cobalt compound nanowires prepared via electrodeposition

Yosuke Asano[a], Toshiki Komatsu[b], Katsuyuki Murashiro[b], Katsuyoshi Hoshino[a,*]

[a] Graduate School of Advanced Integrated Science, Chiba University, 1-33 Yayoi-cho, Inage-ku, Chiba 263-8522, Japan
[b] Goi Research Center, Chisso Petrochemical Corp., 5-1 Goikaigan, Ichihara, Chiba 290-8551, Japan

ARTICLE INFO

Article history:
Received 19 October 2010
Received in revised form 12 January 2011
Accepted 31 January 2011
Available online 5 March 2011

Keywords:
Electrochemical capacitor
Supercapacitor
Nanowire
Nanodendrite
Cobaltous hydroxide
Rapid ion transfer

ABSTRACT

The capacitor properties of cobalt compound nanowire (CCNW) electrodes, prepared by the one-step electroreduction of $[Co(NH_3)_6]^{3+}$ in water, have been investigated. The CCNW electrode changes its various properties during its growth. During the initial growth stage, the CCNW electrodes consist of nanowires with smooth surfaces and have a specific capacitance (C_m) of 310 F g^{-1}. During the middle stage, prickles grow on the CCNW surface, leading to a reduction in its real surface area and its C_m value to 230 F g^{-1}. During the final stage, further growth of the prickles is accompanied by the fusion of the CCNWs, and hence, a drastic decrease in the real surface area. However, a maximum capacitance of C_m = 420 F g^{-1} was obtained during this stage. This unexpected capacitance change was discussed in terms of the effects of rapid ion transfer and the electroactive material/electrolyte interface area. In addition, the aging effect and the cycle life of the CCNW electrode were also investigated.

1. Introduction

Electrochemical capacitors or supercapacitors [1–3] have received a great deal of attention over the past decade because of their high specific capacitance and energy density in comparison to conventional electrical double-layer capacitors (EDLCs) [4], and are expected as candidates for use in the auxiliary power source of hybrid electric vehicles and short-term power source for mobile electronic devices. They are characterized by their charging–discharging reactions based on a Faradaic process, being distinct from a non-Faradaic one involved in the capacitance behavior of the EDCLs. Depending on the materials and the redox reaction mechanism, electrochemical capacitors are classified into two types: one is the use of metal oxides/hydroxides, and the other is based on electrically conducting polymers. In the former material systems, RuO_2 and IrO_2 are considered as the best materials with high energy densities [5–7]. However, their high cost would be a limiting factor for their wide applications. The latter conducting polymer systems [8–10] show a poor durability against redox cyclings for the charging–discharging reactions and have a lower specific capacitance compared to the metal oxides/hydroxides systems. In this context, the cobalt hydroxides/oxides, such as $Co(OH)_2$, CoO_x, and CoOOH, have been the focus as the electrode materials with a high performance [11–19]. Recent reports on these materials have been directed toward the fabrication of nanostructured electrodes consisting of nanoparticles and/or nanoporous materials [13,14,16,18,19]. These structures provide high electrode/electrolyte interface areas and large spaces for the rapid transfer of electroactive species, resulting in high-performance supercapacitors.

On the other hand, we previously proposed a one-step template-free electrochemical method to prepare nanowires consisting of cobalt compounds [20], in which the electrogenerated cobalt compounds were self-organized to form the nanowires. The chemical analyses of the nanowires using energy-dispersive X-ray spectroscopy, X-ray photoelectron spectroscopy, and X-ray diffraction measurements revealed that the nanowires are composed of cobalt hydroxides and cobalt (for simplicity, this nanowire is hereinafter designated a cobalt compound nanowire, CCNW). In addition, this method is characterized by fixing of the CCNWs on the substrate as a film under ordinary pressure and temperature, which would make heating at high temperatures during the film-forming processes useless. These features, combined with the current capacitance studies of cobalt compounds (see above), have stimulated us to investigate the charging–discharging characteristics of the CCNW electrode.

In this paper, we present the first report on the capacitor properties of the CCNW electrodes. The charging–discharging measurements and cyclic voltammetry revealed that they exhibit a high specific capacitance and good recyclability.

* Corresponding author. Tel.: +81 43 290 3478; fax: +81 43 290 3478.
E-mail address: k_hoshino@faculty.chiba-u.jp (K. Hoshino).

0378-7753/$ – see front matter © 2011 Elsevier B.V. All rights reserved.
doi:10.1016/j.jpowsour.2011.01.101

2. Experimental

2.1. Synthesis of CCNWs

The films consisting of the CCNWs were prepared on an indium–tin-oxide coated glass (ITO, 10 Ω sq^{-1}, Geomatech Co.) by the controlled-potential reduction of $[Co(NH_3)_6]Cl_3$ (Aldrich, 99%) at 18 °C [20]. The typical electrolyte solution was prepared by adding $[Co(NH_3)_6]Cl_3$ and 0.1 M Li_2SO_4 (Wako Pure Chemicals, 98%) to distilled-deionized water. The electrodeposition was then carried out using a three-electrode type cell consisting of two compartments immersed in a thermostat (Tokyo Rikakikai Model CTP-01) and a potentiostat (Hokuto-Denko Model HAB-151). The ITO (10 mm × 20 mm × 1.1 mm) and the counter Pt plates (10 mm × 20 mm × 0.3 mm) were immersed in the electrolyte solution (ca. 15 ml) in the main compartment, the distance between the two plates being ca. 1 cm. The area of the ITO exposed to the solution was typically 1.0 cm^2. In the auxiliary compartment (ca. 5 ml) was immersed an agar bridge connected to a reference saturated calomel electrode (SCE, TOA Co.). All the measurements were done under an N_2 atmosphere. After the deposition, the products on the ITO were rinsed with water and then dried in air. The morphology of the CCNW deposits was very much dependent on the added concentration of the $[Co(NH_3)_6]Cl_3$ and the applied potential, E, during the electroreduction [20]. The CCNWs were formed at the added concentration of 19 mM and at $E = -1.03$ V vs. SCE, while the cobalt compound nanodendrites (CCND) were obtained from a 5-mM $[Co(NH_3)_6]Cl_3$ solution by applying −1.2 V vs. SCE to the ITO.

2.2. Electrochemical tests

The electrochemical measurements were carried out in the above three-electrode two-compartment type cell containing LiOH (Wako Pure Chemicals, >98%) aqueous solution. The freshly prepared CCNW on the ITO and a Pt plate were used as the working and the counter electrodes, respectively. All the potentials were referenced to the SCE. Cyclic voltammetry and the charge–discharge tests were conducted using an electrochemical analyzer (BAS Inc., model ALS1200A) and a charge/discharge unit (Hokuto Denko Co., model HJ1010mSM8A), respectively.

2.3. Surface area estimation

The real surface area of the CCNW electrodes was estimated by cyclic voltammetry [21–24]. This technique is available when a rectangular-shaped capacitive current–potential curve (see Fig. 4B) is obtained in a certain potential range. The capacitive current j_{dl} is taken as the average of the anodic (j_a) and cathodic capacitive current (j_c). Using the double layer capacitance (C_{dl}) and sweep rate (ν), j_{dl} is expressed as:

$$j_{dl} = C_{dl}\nu \quad (1)$$

with

$$C_{dl} = \frac{\varepsilon\varepsilon_0 S}{d} \quad (2)$$

where ε, ε_0, S, and d are the relative dielectric constant of the electrolyte solution, the permittivity of free space, real surface area, and double layer thickness, respectively. For the smooth electrode surface, its double layer capacitance can be assumed to be 20 μF cm^{-2} [21,24]. This assumption allows us to estimate the surface roughness factor (r) from the ratio of the C_{dl} value for the CCNW electrode and that for the smooth electrode, $r = C_{dl}/(20\ \mu F\ cm^{-2})$. The surface roughness factor is defined as the ratio of the real surface area to the simple geometric area [25]. However, no rectangular-shaped capacitive current–potential curve was obtained in the cyclic voltammograms of the CCNW electrodes in an aqueous 0.1 M Li_2SO_4 solution due to their high electrochemical activity. Thus, the CCNW electrodes were annealed in air at 500 °C for 1 h and converted to Co_3O_4 nanowire electrodes. This material conversion significantly depressed the redox (or Faradaic) currents to produce the capacitive behavior; the Co_3O_4 nanowire electrode was electrochemically inactive in the potential range of 0.05–0.55 V in an aqueous 0.1 M Li_2SO_4 solution. This behavior allows for the estimation of the C_{dl} for the Co_3O_4 nanowire electrodes. Note that the morphology of the nanowires was only slightly changed by the annealing (see the SEM images of the CCNW and Co_3O_4 nanowires in Supplementary data); hence, the C_{dl} value of the CCNW electrode was regarded as equal to that of the Co_3O_4 nanowire electrode as a first approximation. The details of the material conversion of the CCNWs to the Co_3O_4 nanowires will be reported elsewhere.

2.4. Chemical analyses

The morphology of the CCNWs was investigated by scanning electron microscopic observations (SEM, Topcon ABT-32). Time-of-flight secondary ion mass spectrometry (TOF-SIMS) was employed for the compositional analysis of the CCNWs. The sample for the TOF-SIMS measurements was prepared by placing the CCNWs/ITO samples in ethanol, peeling the CCNWs off the ITO plate by sonication, collecting the CCNWs, and drying. The TOF-SIMS measurements were performed using a TOF.SIMS5 instrument (ION-TOF Co.) equipped with a Bi liquid metal ion gun operating at 25 kV. The analysis area was a 200 μm × 200 μm square. X-ray diffraction (XRD) spectra were obtained with an X-ray diffractometer (Bruker AXS, D8 DISCOVER Highspeed) that used CuKα radiation operating at 45 kV and 360 mA.

3. Results and discussion

3.1. Cyclic voltammetry

Part A in Fig. 1 shows the cyclic voltammograms of the CCNW electrode in an aqueous 0.1 M LiOH solution in the potential range of −1.0 to +0.55 V at the sweep rate of 5 mV s^{-1}. Curves a and b are the first and second sweep waves, respectively. The CCNW electrode was prepared by passing electricity, Q, of 1.0 C cm^{-2}. The potential was initially swept from −0.9 V (rest potential) in the anodic direction, then reversed at 0.55 V. During the forward scan, the irreversible oxidation wave was observed at −0.59 V, which can be assigned to the oxidation of cobalt metal in the CCNW (Eq. (3)) [26]:

$$Co + 2OH^- \rightarrow Co(OH)_2 + 2e^- \quad (3)$$

This wave was not observed in the successive potential scans, indicating that the cobalt metal in the vicinity of the wire surface is completely converted to cobalt hydroxide during the first potential sweep. A large oxidation current then flowed at 0.18 V when the potential was swept in the more anodic direction. However, this large wave was depressed in the second potential sweep (curve b). Part B in Fig. 1 shows the repeated cyclic voltammograms measured in the potential range of 0–0.55 V. After the first potential sweep (curve a, peak potential = 0.18 V), the voltammograms exhibited a pair of redox waves with an anodic peak potential of 0.15 V and a cathodic peak potential of 0.069 V, and is nearly the same in peak shapes and positions as the reported voltammogram of a mesoporous $Co(OH)_2$ film [13,16,17]. It is well accepted that the anodic and the cathodic waves are assigned to the oxidation of $Co(OH)_2$ to

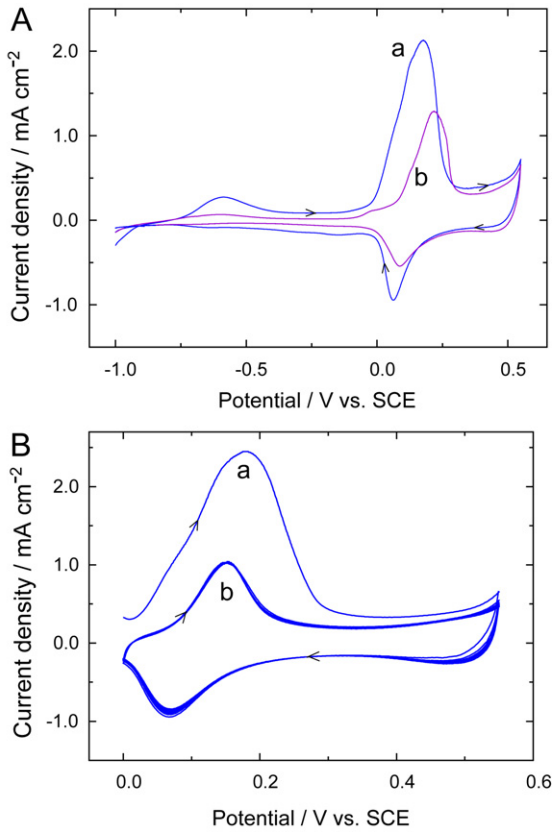

Fig. 1. Cyclic voltammograms of the CCNW electrode in an aqueous 0.1 M LiOH solution at 5 mV s^{-1}. (A) The first (curve a) and the second (curve b) sweep waves in the potential range of −1.0 V to +0.55 V vs. SCE. (B) The first (curve a) and the subsequent repetitive sweep waves (curves b) in the range of 0 V to +0.55 V.

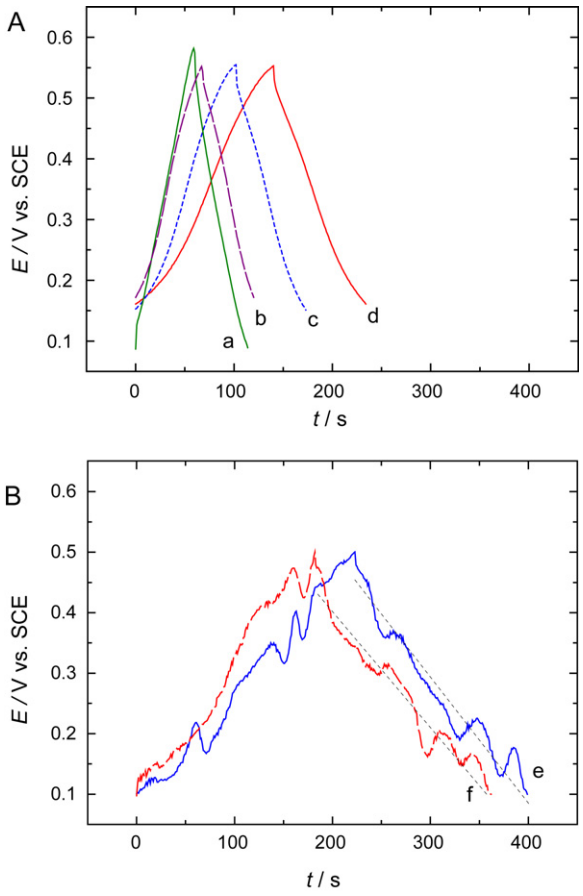

Fig. 2. Constant current density charge/discharge test (potential E–time t curves) for the CCNW electrodes prepared by passing electricity (Q) of 1.0 C cm^{-2} (a), 2.0 C cm^{-2} (b), 3.0 C cm^{-2} (c), and 4.0 C cm^{-2} (d). (B) The CCNW electrodes were prepared at Q = 4.5 C cm^{-2} (e) and 5.0 C cm^{-2} (f).

CoOOH and the reverse process [13,16,17], respectively (Eq. (4)):

$$Co(OH)_2 + OH^- \rightleftharpoons CoOOH + H_2O + e^- \quad (4)$$

Based on these considerations, the high current in the first sweep and its depression after the subsequent sweeps may be accounted for by assuming that the initial surface of the CCNWs involves low oxidation-state cobalt compounds and that they are partially converted to electrochemically inactive species during the first potential sweep. Indeed, the TOF-SIMS measurements of the CCNW revealed that it involves various oxidation-state cobalt compounds as well as cobaltous hydroxide and cobalt metal. Thus, it is conceivable that the anodic wave in curve b in Fig. 1A and the repetitive anodic waves in Fig. 1B (curves b) are assigned to the oxidation of the $Co(OH)_2$ species initially present in the CCNW and those generated from cobalt metal plus the low-oxidation-state cobalt compounds in the first potential sweep. Previous chemical analyses of the CCNW using XPS, EDX, and XRD revealed that the CCNW surface is covered with $Co(OH)_2$, while the CCNW bulk involves cobalt metal [20]. The above electroanalyses, combined with the previous chemical analyses, suggest that the as-grown CCNW deposit involves the $Co(OH)_2$ species, low-oxidation-state cobalt compounds, and cobalt metal. Although the reasons for this hydration are not clear, it is possible that it originates from the corrosion occurring during the handling of the specimens due to the sensitivity of the CCNWs to air and moisture [27]. The experimental data to support this reasoning will be presented in Section 3.4.

The single-electrode specific capacitance, C_m, of the CCNW was estimated from the voltammogram by integrating the cathodic current, $I(E)$, with respect to the potential, E, from the anodic potential limit E_a to the cathodic potential limit E_c and then dividing by the sweep rate (v), the mass of the CCNW deposit (m), and the potential window (E_a–E_c) according to Eq. (5) [12]:

$$C = \frac{1}{mv(E_a - E_c)} \int_{E_c}^{E_a} I(E)dE \quad (5)$$

The capacitance value thus estimated from Fig. 1B was 280 F g^{-1}. In the estimation, E_c and E_a were taken as 0.05 V and 0.55 V, respectively. The value of m was gravimetrically measured to be 1.91×10^{-4} g per 1-cm^2 geometric area of the CCNW electrode prepared at Q = 1.0 C cm^{-2} [20].

3.2. Charging–discharging measurements

In order to highlight the capacitance characteristics of the CCNW, constant current density charge/discharge tests were carried out. Fig. 2 shows the charge and discharge curves, i.e., potential (E)–time (t) response, for the CCNW at a current density of 0.5 mA cm^{-2}. The CCNWs were prepared by passing charges (Q) of 1.0, 2.0, 3.0, 4.0, 4.5, and 5.0 C cm^{-2}. As would be predicted from the results of the cyclic voltammetry in Section 3.1, the initial charging–discharging characteristics were different from the subsequent ones. The curves in Fig. 2 show the typical characteristics measured after the initial charging–discharging experiments. Below Q = 4.0 C cm^{-2} (part A), the E–t responses showed the typical capacitance behavior with a triangular wave shape, indicating that the reversible charging–discharging takes place. On the other hand, oscillating E–t responses were obtained above Q = 4.5 C cm^{-2} (part B). The value of C_m was calculated according to Eq. (6) from

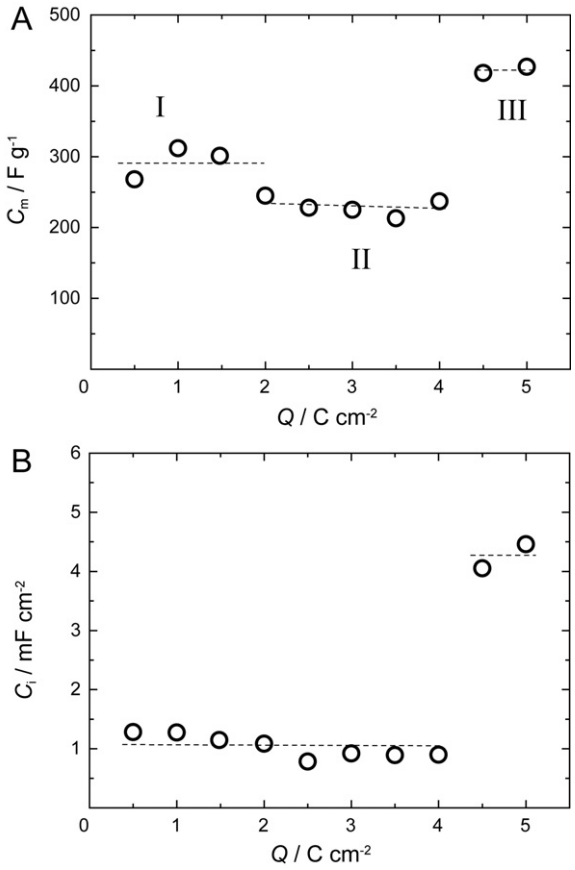

Fig. 3. The dependence of specific capacitance C_m (A) and intrinsic capacitance C_i (B) on Q.

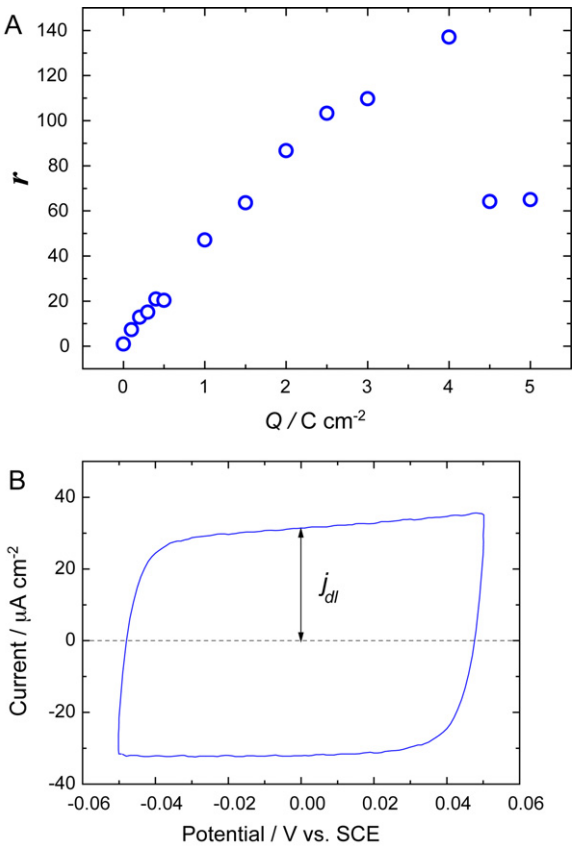

Fig. 4. (A) The dependence of roughness factor (r) of the CCNW electrodes on Q. (B) The typical cyclic voltammogram for measuring the double layer capacitance of the electrode at the sweep rate of 50 mV s^{-1}.

the chronopotentiograms in Fig. 2 [15–17]:

$$C_m = \frac{I \times \Delta t}{\Delta V \times m} \quad (6)$$

where I is the discharge current, Δt is the discharge time, and ΔV is the potential drop during the discharge process. Part A in Fig. 3 shows the dependence of C_m on Q. The dependence can be classified into three regions: (I) slightly higher C_m values were obtained below Q = ca. 2.0 C cm^{-2} and they were nearly independent of Q; (II) the C_m values are relatively low and nearly independent of Q in the range of 2.0 C cm^{-2} < Q < 4.0 C cm^{-2}; (III) the C_m values are relatively high beyond Q = ca. 4.0 C cm^{-2}. The C_m value at Q = 1.0 C cm^{-2} agrees well with the specific capacitance derived from the cyclic voltammetry (see Section 3.1). At Q = 4.5 and 5.0 C cm^{-2}, the C_m values were roughly estimated from the dotted lines in Fig. 2B due to the oscillation behavior of the E–t curves.

In order to understand the above complicated C_m–Q relationship, we have to consider the key factors affecting the capacitance of the electrochemical capacitors with specific nanostructures. The factors involve a rapid ion transfer and high electroactive material/electrolyte interface area [13,14,16,17,28]. Many researchers have devised various nanoporous structures and channels to improve the ion transfer rate during the charging–discharging process and to increase the real surface area at the electroactive material/electrolyte interface. In order to investigate these factors in our specific nanowire system, surface area measurements (see Section 2.3) and scanning electron microscopic (SEM) observations were carried out on the CCNW electrodes. Part A in Fig. 4 shows the dependence of the roughness factor (r) on Q for the CCNW electrodes. Part B is a typical example of the cyclic voltammogram for measuring the double layer capacitance. The sample is the Co_3O_4 deposit electrode prepared at Q = 1.0 C cm^{-2}. The reason for the use of the Co_3O_4 deposit electrode instead of the CCNW deposit has already been described in Section 2.3. The j_{dl} value of this voltammogram gives r = 50 which corresponds to 26 m^2 g^{-1}. The r value linearly increased with an increase in Q below Q = ca. 2.0 C cm^{-2}, indicating that no loss in the real surface area is accompanied by the growth of the nanowires (e.g., losses due to growth in the radial direction, overlapping, fusion, and destruction of the wires). This is compatible with the SEM observations of the CCNW electrodes (Fig. 5). The morphology of the CCNW electrode prepared at Q = 1.0 C cm^{-2} (image a) was nearly the same as that at Q = 2.0 C cm^{-2} (image b), implying that the nanowires grow such that their real surface area linearly increases with Q. This morphological feature should form the basis of the relatively high and constant C_m values obtained in this Q region (region I in Fig. 3A).

In the region of ca. 2.0 C cm^{-2} < Q < 4.0 C cm^{-2}, the r value gradually increased in such a way that the rate of increase tapers off. Parts c and d in Fig. 5 show the SEM images of the CCNW electrodes prepared at Q = 3.0 and 4.0 C cm^{-2}, respectively. Prickles were grown on the nanowire surface. The consequence was that the wires grew thicker. This indicates that the electrolysis current for the deposition of the cobalt compounds does not effectively contribute to the enlargement of the real surface area, and accounts for a slowdown in r in region II. The values of C_m in this region tend to slightly decrease with Q, but can be regarded as nearly independent of Q, suggesting that the effect of the prickles is not very high.

Beyond Q = 4.0 C cm^{-2}, a drastic change in the morphology was observed (parts e and f in Fig. 5). Further growth of the prickles occurred, which was accompanied by a decrease in the real surface area to ca. 50% of that at Q = 4.0 C cm^{-2} probably due to the overlapping and fusion of the nanowires through the prick-

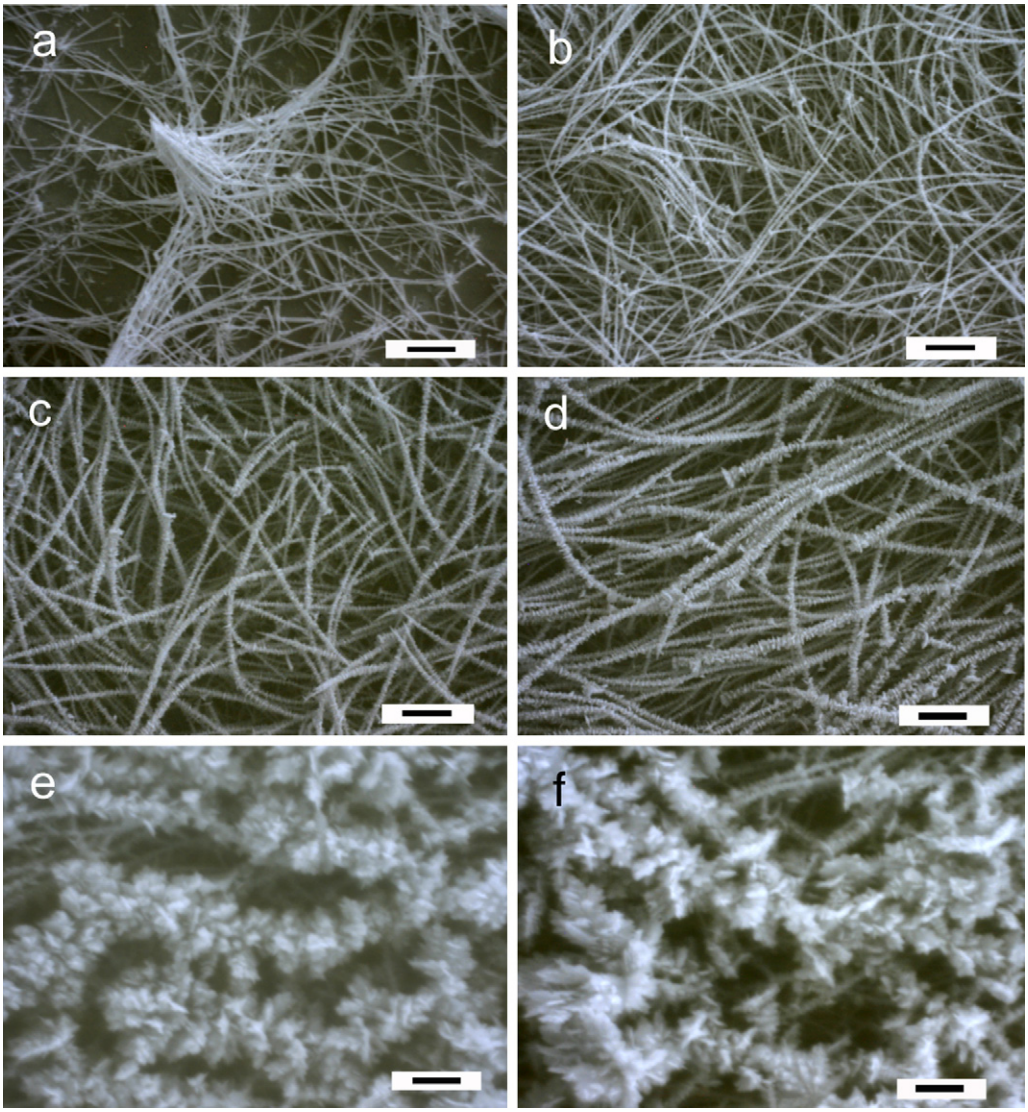

Fig. 5. SEM images of the CCNWs prepared at $Q = 1.0\,C\,cm^{-2}$ (a), $2.0\,C\,cm^{-2}$ (b), $3.0\,C\,cm^{-2}$ (c), $4.0\,C\,cm^{-2}$ (d), $4.5\,C\,cm^{-2}$ (e), and $5.0\,C\,cm^{-2}$ (f). Scale bars: 10 μm.

les structures. In this region of Q (region III), the value of C_m is greater than those in regions I and II. This region is characterized by a potential oscillation in the charging–discharging plots. It is likely to assume that the above-described overlapping and fusion of the nanowires result in the division of the CCNW electrode into small spaces, in which the rapid transfer of OH^- ions is made possible since the distance over which the ions have to travel is quite small. The increase in C_m by the effect of this rapid ion transfer may overwhelm the decrease in C_m by the effect of the decrease in r, resulting in the relatively higher values of C_m in region III. However, in such a small space, the depletion of the OH^- ions and their supply from the solution bulk may alternatively occur during the charging–discharging reactions. During the charging process, on the basis of Eq. (4), the depletion of the OH^- ions leads to an increase in the electrode potential and their subsequent supply causes a decrease in the potential. The potential oscillation in Fig. 2 might be explained on this basis. In order to confirm this potential oscillation model, the concentration of LiOH was increased from 0.1 M to 1 M and the charging–discharging behavior of the CCNW electrode was investigated. Fig. 6 shows the discharge curves for the CCNW electrodes prepared at $Q = 4.5\,C\,cm^{-2}$ (curves a and b) and $Q = 5.0\,C\,cm^{-2}$ (curves c and d) in aqueous 0.1 M (curves a and

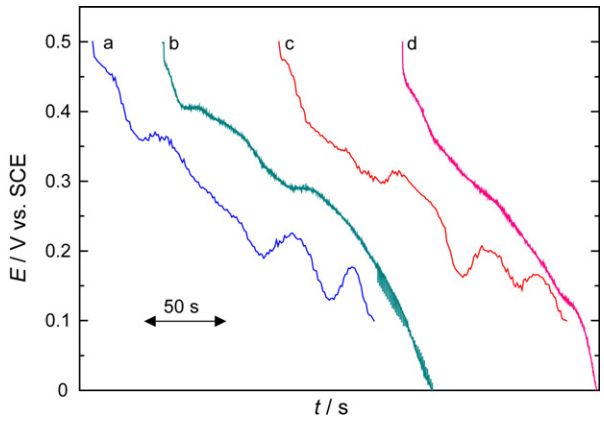

Fig. 6. The effect of the LiOH concentration on the shape of the discharge curves for the CCNW electrodes prepared at $Q = 4.5\,C\,cm^{-2}$ (curves a and b) and $Q = 5.0\,C\,cm^{-2}$ (curves c and d). The curves were recorded in aqueous 0.1 M (curves a and c) and 1 M LiOH (curves b and d) solutions.

Table 1
Specific capacitance (C_m) and roughness factor (r) for the CCNW and CCND electrodes.

Property	CCNW[a]	CCND[a]
C_m (F g^{-1})	310[b]	181[b]
	280[c]	218[c]
r	47	25

[a] Prepared by passing electricity of $Q = 1.0$ C cm^{-2}.
[b] Measured by charge/discharge test.
[c] Measured by cyclic voltammetry.

c) and 1 M LiOH (curves b and d) at a current density of 0.5 mA cm^{-2}. In agreement with our expectation, the oscillation amplitude of the potential was significantly diminished by increasing the concentration of LiOH, thus supporting the potential oscillation model based on the mass transfer limitation in a small nanospace.

The value of C_m involves the electric double-layer capacitance C_{dl}, which can be calculated using the intrinsic capacitance for the smooth electrode surface, 20 μF cm^{-2}, and the real surface area shown in Fig. 4. The calculation gave the contribution of the double-layer capacitance of $C_{dl} = 5.2$ F g^{-1} for the CCNW electrode prepared at $Q = 1.0$ C cm^{-2} ($C_m = 310$ F g^{-1}). Thus, the pseudo capacitance based on the Faradaic process (Eq. (4)), C_m^F, was estimated as the difference between C_m and C_{dl}, i.e., 305 F g^{-1}. If we assume that the CCNW is only composed of $Co(OH)_2$, the fraction of the $Co(OH)_2$ that contributes to the charging–discharging, f, can be calculated using Eq. (7) [12]:

$$f = \frac{C_m^F \times M \times \Delta V}{F} \quad (7)$$

where M is the molecular weight of $Co(OH)_2$, ΔV is the potential window, and F is the Faraday constant. The value of f was calculated to be 0.15 using $C_m^F = 305$ F g^{-1} for $Q = 1.0$ C cm^{-2}, $\Delta V = 0.5$ V, and $M = 92.9$ g mol^{-1}. This result indicates that 15% of the $Co(OH)_2$ contributes to the charge storage and implies that the electrochemical events are not restricted to the surface $Co(OH)_2$ species [12]. However, this conclusion is tentative since the electrochemically inactive species may be involved in the CCNW after the initial potential-sweep treatment (see Section 3.1). Instead, the bulk contribution was confirmed by estimating the single-electrode intrinsic capacitance, C_i (F cm^{-2} of real surface area). Using the r values in Fig. 4 and the C_m values in Fig. 3A, C_i was calculated. Part B in Fig. 3 shows the plot of C_i vs. Q. The C_i values are in the range of ca. 1–4.5 mF cm^{-2}, being much greater than that expected for EDLC, ca. 20 μF cm^{-2}, and therefore, being the indication of bulk utilization. The dependence of C_i on Q is classified into two regions, i.e., below and above $Q = 4.0$ C cm^{-2}. The former region, in which C_i is nearly independent of Q, implies that the capacitance is determined solely by the real surface area. On the other hand, the higher capacitance values of the latter region may be affected by the rapid ion transfer as already described.

3.3. CCND electrode

In the previous section, it was suggested that the capacitance of the CCNW electrodes was mainly determined by their real surface area in the region of $Q < 4.0$ C cm^{-2}. In order to confirm this suggestion, the CCND electrode was prepared at $Q = 1.0$ C cm^{-2} (see Section 2.1) and its C_m value was measured together with its r value. Its SEM image (part A in Fig. 7) revealed that nanorod structures aggregate into leaf-like forms called dendrites. The intimate contact among the nanorods implies its smaller real surface area compared with that of the CCNW. Indeed, its r value is 53% of that for the CCNW electrode (Table 1). The solid line in Fig. 7B shows the charging–discharging curve for the CCND electrode. For comparison, the curve for the CCNW electrode was also included in the figure (dotted curve). The C_m value of the CCND electrode, determined by chronopotentiometry, was 58% of that of the CCNW electrode (Table 1). Such a decrease in C_m with r may be more support for the capacitance behavior described in Section 3.2.

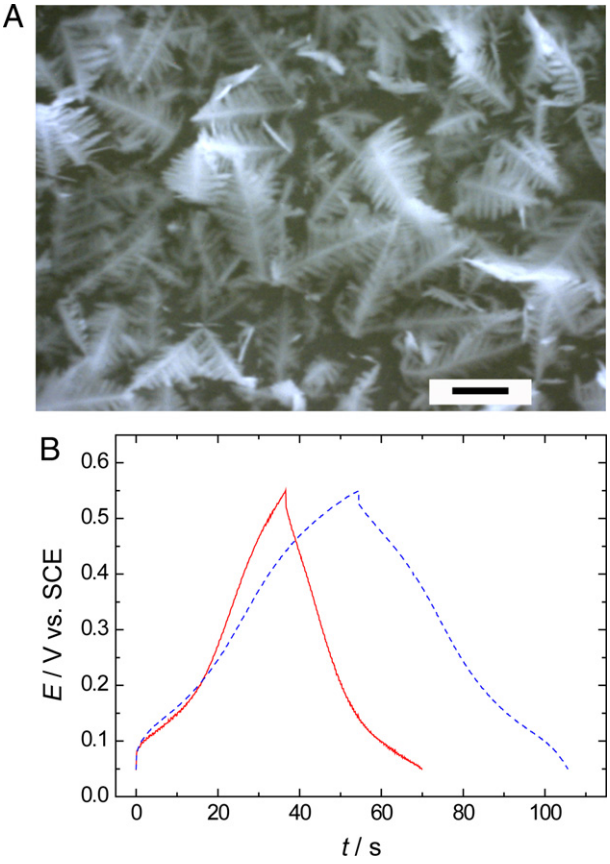

Fig. 7. (A) SEM image of the CCND electrode. Scale bar: 2 μm. (B) The charging–discharging curves of the CCND electrode (solid curve). The curve for the CCNW electrode (dotted curve) is also included for comparison purposes. Both electrodes were prepared at $Q = 1.0$ C cm^{-2}.

3.4. Aging of CCNW electrodes

The CCNW electrodes showed aging after their electrochemical synthesis, so that the C_m values were measured at selected times during their storage under atmospheric conditions of 22 °C and 50%RH. The electrodes were prepared by passing 1.0 C cm^{-2} electricity. Part A in Fig. 8 shows the dependence of C_m on the aging time, t_a, which was taken as the time after the synthesis. The C_m value initially increased with t_a and reached a steady state value of 310 F g^{-1} in ca. 2 h. As described in Section 3.1, the chemical species responsible for the charging–discharging is cobaltous hydroxide, and the as-grown CCNW involves cobaltous hydroxide, cobalt metal, and low-oxidation-state cobalt compounds in the vicinity of its surface. Based on these findings, it is likely that the partial conversion of the cobalt metal and low-oxidation-state cobalt compounds to cobaltous hydroxide is caused during the aging process and led to the increase in C_m with t_a. Based on this aging effect, the CCNW and CCND electrodes employed in Sections 3.1–3.3 had been stored under atmospheric conditions of 22 °C and 50%RH for more than 2 h prior to their use. Fig. 9 is the X-ray diffraction (XRD) patterns of the CCNW electrodes prepared at $Q = 1.0$ C cm^{-2} (a), 3.0 C cm^{-2} (b), and 5.0 C cm^{-2} (c). The peaks at $2\theta = 41.51$, 44.47, and 47.36 can be indexed as hexagonal Co (JCPDS 05-0727). Trace cobaltous hydroxide peaks (JCPDS 74-1057)

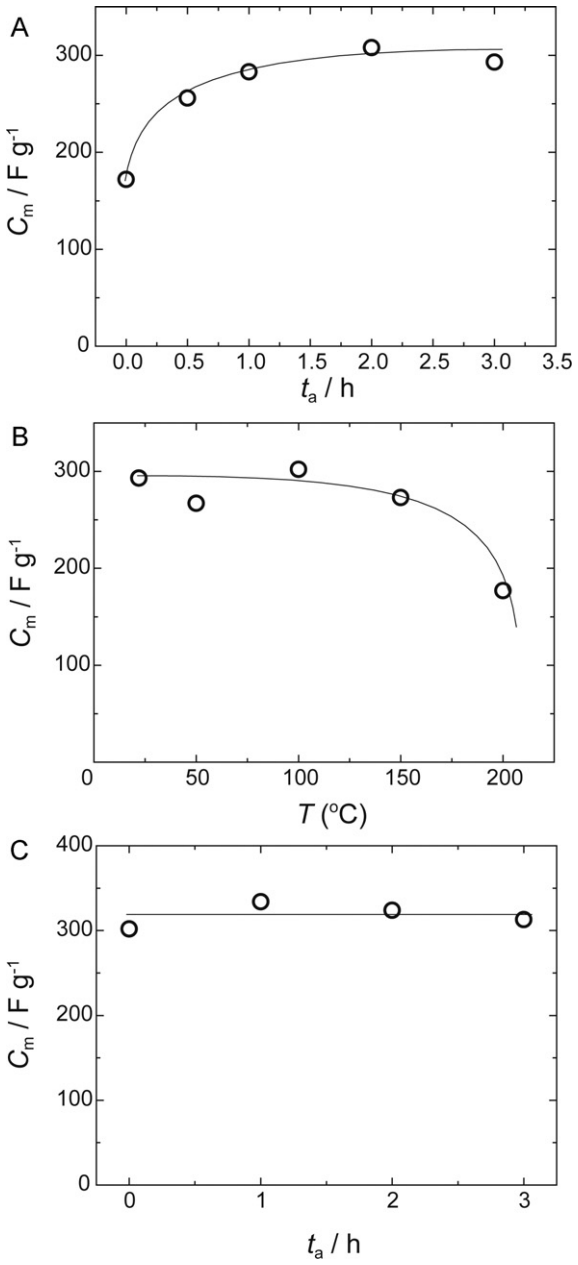

Fig. 8. (A) The dependence of C_m on aging time, t_a. The CCNW electrodes, prepared at $Q = 1.0\,C\,cm^{-2}$, were stored in air (22 °C, 50%RH) for a selected aging time. (B) The dependence of C_m on the annealing temperature, T, for investigating the thermal stability of the CCNW electrode ($Q = 1.0\,C\,cm^{-2}$). (C) The dependence of C_m on t_a for the CCNW electrodes prepared at $Q = 1.0\,C\,cm^{-2}$ and annealed at $T = 100$ °C for 1 h.

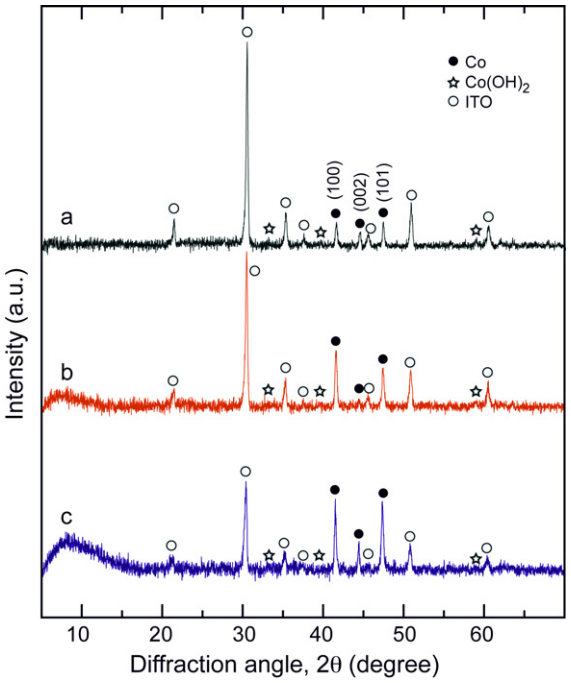

Fig. 9. XRD patterns of the CCNW electrodes prepared at $Q = 1.0$ (a), 3.0 (b), and $5.0\,C\,cm^{-2}$ (c).

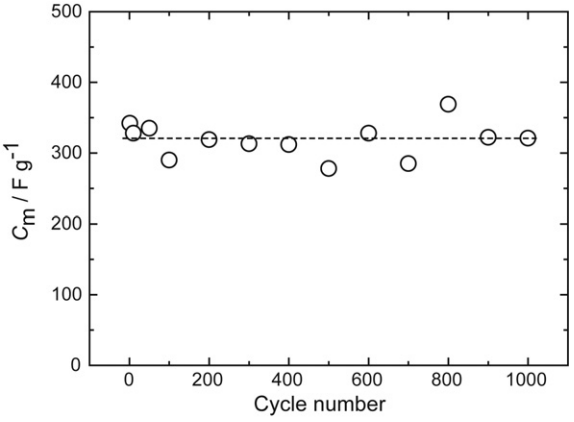

Fig. 10. The C_m value of the CCNW electrode ($Q = 1.0\,C\,cm^{-2}$) in 0.1 M LiOH as a function of the cycle number. The current density was $0.5\,mA\,cm^{-2}$.

can also observed in the CCNW deposit prepared at $1.0\,C\,cm^{-2}$. However, these peaks are less pronounced at $Q = 3.0\,C\,cm^{-2}$ and negligibly small at $Q = 5.0\,C\,cm^{-2}$. This can be explained by assuming that the thickness of the cobaltous hydroxide layer on the wire surface is nearly constant regardless of Q, and therefore, its contribution to the total amount of the CCNW deposit decreases with Q. This result may be another support for our reasoning concerning the chemical structure of the CCNW electrodes (see Section 3.1). The next concern is the stability of the steady-state CCNW electrodes to the ambient temperature. Hence, the steady-state CCNW electrodes were annealed at various temperatures for 1 h and their C_m values were measured by the charging–discharging measurements. Part B in Fig. 8 shows the dependence of C_m on the annealing temperature, T. The CCNW electrode was found to be thermally stable below ca. 150 °C. This temperature is in good agreement with the one at which the thermal transformation of $Co(OH)_2$ to CoOOH and Co_3O_4 occurs [29]. The annealed CCNW electrodes showed no aging. For example, the C_m value of the CCNW electrode annealed at 100 °C was unchanged during its storage in air (part in Fig. 8).

The electrochemical stability of the CCNW electrode was examined in a 0.1 M LiOH aqueous solution by charging–discharging cycling at a current density of $0.5\,mA\,cm^{-2}$. The electrode was prepared at $Q = 1.0\,C\,cm^{-2}$ and aged in air (22 °C, 50%RH) for more than 2 h. As shown in Fig. 10, the values of C_m were nearly the same during 1000 consecutive cycles, indicating the excellent long-term electrochemical stability of the CCNW electrode and, consequently, no degradation of the nanowire structure.

4. Conclusions

The electrochemical characterization of the cobalt compound nanowire (CCNW) electrodes and their capacitance studies were carried out. The cyclic voltammetric measurements of the CCNW

electrode suggested that the as-grown CCNW involves cobaltous hydroxide, cobalt metal, and low-oxidation-state cobalt compounds in the vicinity of its surface, and that the cobalt metal and a part of the low-oxidation-state compounds are converted to cobaltous hydroxide by the electrochemical treatment in an aqueous 0.1 M LiOH solution (Section 3.1). The charging–discharging characteristics of the CCNW electrodes were investigated by varying the amount of electricity passed during the electrosynthesis of the CCNW electrodes, Q (Section 3.2). The specific capacitance, C_m, was very dependent on Q (Section 3.2). The C_m values of 310, 230, and 420 F g^{-1} were obtained in the regions of Q below 2.0 C cm^{-2}, between 2.0 C cm^{-2} and 4.0 C cm^{-2}, and above 4.0 C cm^{-2}, respectively. This dependence of C_m on Q was closely related to the change in morphology of the CCNW with Q, and was explained by the effects of rapid ion transfer in the nanospaces and the change in real surface area with Q. The intrinsic capacitance, C_i, was also investigated as a function of Q. The investigation revealed that the charging–discharging events are not restricted to the surface $Co(OH)_2$ species, and suggested that the effect of rapid ion transfer is significant above 4.0 C cm^{-2}. The cobalt compound nanodendrite (CCND) electrode also exhibited a capacitor behavior; however, its C_m value (181 F g^{-1}) was lower than that of the CCNW electrode (310 F g^{-1}), being in accordance with the smaller real surface area of the former than the latter (Section 3.3). The CCNW electrode showed aging during its storage in air and its C_m value increased from 150 F g^{-1} to 310 F g^{-1} in ca. 2 h after its electrosynthesis (Section 3.4). The aging was explained by an increase in the amount of the $Co(OH)_2$ species with storage time. The cycle life of the CCNW electrode was stable for one thousand cycles.

Acknowledgement

The authors thank MOBARA ATECS Ltd. for the TOF-SIMS data.

Appendix A. Supplementary data

Supplementary data associated with this article can be found, in the online version, at doi:10.1016/j.jpowsour.2011.01.101.

References

[1] Yu.M. Vol'fkovich, T.M. Serdyuk, Russ. J. Electrochem. 38 (2002) 1043–1068.
[2] P. Simon, Y. Gogotsi, Nat. Mater. 7 (2008) 845–854.
[3] Y. Zhang, H. Feng, X. Wu, L. Wang, A. Zhang, T. Xia, H. Dong, X. Li, L. Zhang, Int. J. Hydrogen Energy 34 (2009) 4889–4899.
[4] A.G. Pandolfo, A.F. Hollenkamp, J. Power Sources 157 (2006) 11–27.
[5] J.P. Zheng, P.J. Cygan, T.R. Jow, J. Electrochem. Soc. 142 (1995) 2699–2703.
[6] C.-C. Hu, W.-C. Chen, K.-H. Chang, J. Electrochem. Soc. 151 (2004) A281–A290.
[7] K. Naoi, S. Ishimoto, N. Ogihara, Y. Nakagawa, S. Hatta, J. Electrochem. Soc. 156 (2009) A52–A59.
[8] D. Villers, D. Jobin, C. Soucy, D. Cossement, R. Chahine, L. Breau, D. Bélanger, J. Electrochem. Soc. 150 (2003) A747–A752.
[9] K. Machida, Y. Nakagawa, N. Ogihara, K. Naoi, Electrochemistry 73 (2005) 1035–1041.
[10] Li-Z. Fan, J. Maier, Electrochem. Commun. 8 (2006) 937–940.
[11] C. Lin, J.A. Ritter, B.N. Popov, J. Electrochem. Soc. 145 (1998) 4097–4103.
[12] V. Srinivasan, J.W. Weidner, J. Power Sources 108 (2002) 15–20.
[13] L. Cao, F. Xu, Y.-Y. Liang, H.-L. Li, Adv. Mater. 16 (2004) 1853–1857.
[14] E. Hosono, S. Fujihara, I. Honma, M. Ichihara, H. Zhou, J. Power Sources 158 (2006) 779–783.
[15] C. Yuan, X. Zhang, B. Gao, J. Li, Mater. Chem. Phys. 101 (2007) 148–152.
[16] W.-J. Zhou, D.-D. Zhao, C.-L. Xu, H.-L. Li, Electrochim. Acta 53 (2008) 7210–7219.
[17] Z. Hu, L. Mo, X. Feng, J. Shi, Y. Wang, Y. Xie, Mater. Chem. Phys. 114 (2009) 53–57.
[18] V. Gupta, S. Gupta, N. Miura, J. Power Sources 177 (2008) 685–689.
[19] T. Zhao, H. Jiang, J. Ma, J. Power Sources 196 (2011) 860–864.
[20] K. Hoshino, Y. Hitsuoka, Electrochem. Commun. 7 (2005) 821–828.
[21] R. Karimi Shervedani, A. Lasia, J. Appl. Electrochem. 29 (1999) 979–986.
[22] R.K. Shervedani, A. Lasia, J. Electrochem. Soc. 145 (1998) 2219–2225.
[23] F. Švegl, B. Orel, I. Grabec-Švegl, V. Kaučič, Electrochim. Acta 45 (2000) 4359–4371.
[24] M. Popczyk, A. Budniok, A. Lasia, Int. J. Hydrogen Energy 30 (2005) 265–271.
[25] H.J. Oha, G.-S. Park, J.-G. Kimc, Y. Jeong, C.-S. Chie, Mater. Chem. Phys. 82 (2003) 331–334.
[26] A. Yuan, S. Cheng, J. Zhang, C. Cao, J. Power Sources 77 (1999) 178–182.
[27] H. Cao, Z. Xu, H. Sang, D. Sheng, C. Tie, Adv. Mater. 13 (2001) 121–123.
[28] V. Khomenko, E. Frackowiak, F. Béguin, Electrochim. Acta 50 (2005) 2499–2506.
[29] T.N. Ramesh, J. Solid State Chem. 183 (2010) 1433–1436.